Effects of Known and Unknown Antenna Position Errors on MVDR

Bailey Miller
Aerospace Engineering
University of Kansas
Lawrence, KS
BaileyJMiller@ku.edu

Brandon Randolph
Center for Remote Sensing of Ice Sheets
University of Kansas
Lawrence, KS
brandon.randolph@ku.edu

John Paden
Center for Remote Sensing of Ice Sheets
University of Kansas
Lawrence, KS
paden@ku.edu

Emily Arnold
Aerospace Engineering
University of Kansas
Lawrence, KS
earnold@ku.edu

***Abstract*—We assess the impact of known and unknown position errors on two variations of the Minimum Variance Distortionless Response (MVDR) algorithm specifically for measurements using multipass, swarms or constellations that involve non-rigid and varying sensor offsets. We consider this in the context of the radar systems and autonomous aircraft used by Center for the Remote Sensing of Ice Sheets (CReSIS) for conducting measurements of snow and ice in polar regions. We find that unknown position errors affect all algorithms in a uniform way and that the performance impact is not related to known position errors. We also find that MVDR is largely unaffected by known position errors except when the number of elements is small. However, self-nulling can result in substantially worse performance than even the simple non-adaptive periodogram method.**

***Index Terms*—array signal processing, array calibration, MVDR, radar clutter**

I. Introduction

Modern remote sensing applications use beamforming algorithms to increase the Signal to Noise Ratio (SNR) of the received signal in the presence of clutter and other interfering signals. At the Center for the Remote Sensing of Ice Sheets (CReSIS), we have developed several airborne radar systems with multichannel arrays to sound ice sheets in polar regions [1]. During data processing, beamforming algorithms are effective tools to reduce surface clutter produced from rough ice surfaces at off-nadir angles [2]–[5]. Surface clutter is undesired backscatter signals from the rough ice surface at off-nadir angles which can mask the return signal from the bedrock at nadir.

The ice sounding community is assessing the efficacy of multipass beamforming measurements with a single platform or a single pass beamforming measurement on multiple platforms, such as an Unmanned Aerial System (UAS) swarm or a constellation of nanosatellites [6]–[8]. Multipass measurements for beamforming are useful when the antennas or required baselines are so large that it is impractical to install the elements on a single platform. Swarms and constellations of UAS are gaining popularity because of their increasing capability and lower costs as compared to larger vehicles capable of carrying multiple antenna elements.

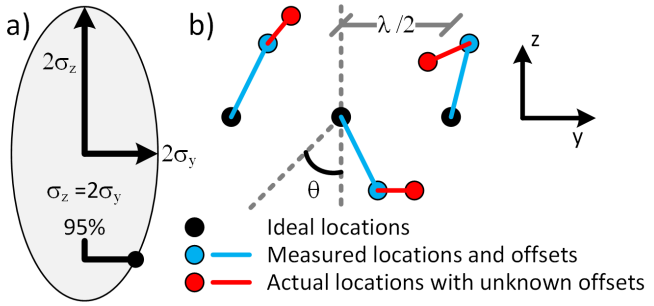

Fig. 1: a. Offset standard deviations and b. array and offset geometry.

In realistic constellation scenarios (multipass, swarm or satellite), we may have relatively large offsets from our desired position that we can measure with GPS. We define these offsets as the *measured offset*. The error in the measured offsets (due to GPS errors) are the *unknown offset*. Figure 1 illustrates these offsets for a simple three-element array and the typical offset relationship between vertical and horizontal components with the ellipse showing this in two dimensions. As an example, most manufacturers quote post processed GPS errors, which constitute the *unknown offset*, as having vertical errors (5-10 cm) twice that of horizontal errors (2-5 cm). Similarly, using the fixed-wing 85 lb. UAS that was developed and operated by researchers at KU [6], we found that the measured and therefore *known offsets* for this UAS flight controller were approximately twice as large in the vertical dimension ($z = 2.01$ m) as in the horizontal dimension ($y = 1.21$ m).

We seek to understand how precisely the flight control and subsequent relative trajectory estimations need to be to achieve a certain level of system performance. We consider each offset type independently and the interplay between the two. By forming a simulated phased array from independent flying elements, we can examine the performance of this array using the algorithms that CReSIS currently applies to ice sounding radar.

The effects of position errors on array processing have been studied extensively in the literature (e.g. [9], [10]).

Several works study wing flexure position errors to understand the effects on sidelobe performance [11], [12] and direction finding accuracy [13], but do not consider the particular variations of Minimum Variance Distortionless Response (MVDR) employed for ice sounding radar. [14] discusses position errors for a UAS swarm, but only provides a single example pattern. Generally, previously published work considers known errors or unknown errors, but not both simultaneously. One exception is [15], which provides a large set of simulations; however, in this work the individual radiation patterns are presented for each run, which are hard to interpret compared to the expectation of the SNR that we use in our results. Also, only 10% of a wavelength (λ) in error is considered rather than a range of errors.

This paper is organized as follows. In Section II, we describe the signal model, model parameters, and performance metrics to understand how array position errors affect performance. We also provide descriptions of each of the beamforming algorithms that are compared. In Section III, we illustrate the effect of position errors on the algorithms using computer simulations over typical ranges of system parameters. Our concluding remarks are given in Section IV.

II. Methodology

The signal model for an array with P sensors or antenna elements, Q narrow-band sources or targets, and M snapshots is shown in Equation 1. $\mathbf{X}$ is the P by M measured signal matrix where each column is one snapshot; $\mathbf{A}$ is the P by Q steering vector matrix where each column represents the steering vector for a corresponding source; $\mathbf{S}$ is the Q by M source signal matrix where each row represent the M snapshots for a particular source; and $\mathbf{N}$ is the P by M noise matrix. The narrow-band assumption allows the source signal variations across the sensors to be modeled in Equation 1 by a single complex number in $\mathbf{A}$.

$$\mathbf{X} = \mathbf{AS} + \mathbf{N}. \tag{1}$$

The modeled sources and noise are independent and identically distributed zero mean complex Gaussian random vectors. The sources and noise are all independent of one another as well. The M snapshots are independent and stationary. The sensors are assumed to be isotropic and unity gain, so the model is only dependent on the relative positions of the sensors. In our ice sounding application, these assumptions are violated to varying degrees, but this simple model is used as a first order approximation.

The output of the array is given by $\vec{w}^H\mathbf{X}$ where H is the Hermitian operator. The filter weights $\vec{w}$ form a P element column vector. The determination of the filter weights is described in the following subsections. For the data adaptive filters, the weights are formed using a Data Covariance Matrix (DCM) estimated from the signal measurement snapshots, $\mathbf{X}$. For non-adaptive filters, the filter weights do not depend on the snapshots.

The sensor positions are modeled with an ideal P-element Uniform Linear Array (ULA) with half wavelength sampling located at $z = 0$ as shown in Figure 1b. Then we add the *measured offsets* to obtain the *measured positions*. Finally, we add the *unknown offsets* associated with the measurement error to obtain the *actual positions*. The actual positions will be used to form the steering vector $\mathbf{A}$ in the signal model of Equation 1 to create simulated snapshots. The measured positions (as opposed to the actual positions) will be used by beamforming algorithms to generate the filter weights, $\vec{w}$. The measured and unknown offsets are modeled by zero mean elliptical Gaussian random variables. The y and z position errors are assumed to be independent. The measured offsets $(\Delta_{y\ meas},\ \Delta_{z\ meas})$ and unknown offsets $(\Delta_{y\ unk},\ \Delta_{z\ unk})$ are independent of each other.

All element offsets are expressed in units of percent wavelength $(\%\lambda)$ so that the results are frequency independent. It is important to note that along-track offsets (x-axis) are not investigated within this paper, because errors in this axis are mitigated during the Synthetic Aperture Radar processing stage, which is not discussed in this work.

The steering vector for source $q \in \{1, \ldots, Q\}$ which forms the q^{th} column of $\mathbf{A}$, denoted as $\mathbf{A}_q$, is generated from the actual sensor positions, $(y_p,\ z_p)$ for $p \in \{1, \ldots, P\}$, and the direction of arrival, θ_q and can be expressed as

$$\mathbf{A}_q = e^{jk(-y_p \sin\theta_q - z_p \cos\theta_q)}, \tag{2}$$

where $k = 2\pi/\lambda$ is the wavenumber. The beam pattern for weight vector $\vec{w}$ evaluated as a function of the direction of arrival θ is

$$AF(\theta) = \sum_{p=1}^{P} w_p^*\ e^{jk(-y_p \sin\theta - z_p \cos\theta)}, \tag{3}$$

where $*$ represents conjugation.

In order to evaluate the performance of each algorithm's tolerance to known and unknown position errors, we choose parameter ranges that match our ice sounding application. In all experiments, we generate results for 20, 100, and 1000 snapshots. The typical number of snapshots in ice sounding generally ranges from 10 to 100, in order to ensure stationarity of the snapshots. Most CReSIS antenna arrays use between three and eight elements so we have chosen to simulate with $P = 3$ and $P = 8$ elements to match the currently deployed arrays and what we also consider to be a reasonable number of passes to collect for the multipass problem under consideration.

Simulations in this study have one clutter source, $Q = 2$, unless specifically noted otherwise in which case there are two clutter sources, $Q = 3$. The desired source is always source $q = 1$ and is at broadside or $\theta = 0°$. The interferers are fixed at $\theta = 45°$ from broadside with one clutter source and $\theta = \pm 45°$ from broadside for two clutter sources. Typical surface clutter in ice penetrating radar arrives from one or both sides of the aircraft and ranges from $30°$to $80°$. For all simulations, the variance is unity for both desired and clutter sources, and the noise variance is 0.1.

The simulated random position offsets, $(\Delta_{y\ meas},\ \Delta_{z\ meas})$ and $(\Delta_{y\ unk},\ \Delta_{z\ unk})$, have a vertical

standard deviation (σ_z) twice that of the horizontal standard deviation (σ_y) as shown in Figure 1. This relationship between vertical and horizontal errors is consistent with the GPS position errors quoted by most GPS receiver manufacturers; GPS is the primary means of measuring the position for our application. As noted in the introduction, CReSIS's measured flight controller trajectory accuracy has a similar relationship between horizontal and vertical errors. In the results of this paper, offsets always represent 2σ so that about 95% of the offsets will have a magnitude, (e.g. $(\Delta_{y\ unk}^2 + \Delta_{z\ unk}^2)^{0.5}$), less than the corresponding $\%\lambda$.

The performance parameter used for comparison throughout this paper is SNR, and it is calculated after each run of a given processing case. The SNR is found by taking the sum of the signal power from all M snapshots and dividing this by the sum of the noise power from all M snapshots. The equation used to calculate SNR for a single run with M snapshots is shown in Equation 4. In the equation, $\mathbf{A}_1$ is the P length steering vector of the desired source at nadir, $\vec{s}_{1,m}$ is the m^{th} snapshot of the desired source, $\mathbf{A}_{2:Q}$ represents the P by $Q-1$ steering vector matrix corresponding to the $Q-1$ clutter sources, the m^{th} snapshot of the clutter sources is the $Q-1$ length vector $s_{2:\vec{Q},m}$, and the m^{th} snapshot of the noise for each channel is $\vec{n}_m$.

$$SNR = \frac{\sum_{m=1}^{M} |\vec{w}^H \mathbf{A}_1 s_{1,m}|^2}{\sum_{m=1}^{M} |\vec{w}^H (\mathbf{A}_{2:Q} \vec{s}_{2:Q,m} + \vec{n}_m)|^2}. \quad (4)$$

The given SNR equation calculates the SNR for a single run. The SNR from each run is then averaged in the log domain, which is the result that is presented. Each data point presented is generated from the average of 1000 runs to obtain an accurate expected value. This number of runs is selected because the computing time is reasonable and the resulting data appears to be consistent and smooth enough for interpretation.

The beamforming algorithms investigated include the periodogram with a Dolph-Chebyshev window, and two versions of the MVDR algorithm. The periodogram technique will provide a performance baseline to compare the two MVDR algorithms against. These two algorithms are the primary clutter reduction methods that CReSIS uses [2]. The beamforming algorithms are briefly described in the next three subsections.

A. Case 1: Periodogram with Chebyshev Window

The data-independent periodogram weights are the component-wise multiplication of the 30 dB sidelobe Dolph-Chebyshev window with phase corrections based on the *measured offsets*. The periodogram with a window is often called the *modified periodogram*. No correction is applied to the amplitude weights, even if the measured offsets are large enough to cause the ordering of the antenna elements along the y-axis to change. Note that the periodogram refers to the average power of the filter output which is what forms the radar image. However, we present the filter SNR before power detection and averaging of snapshots.

A representative array factor plot is shown in Figure 2a. Each of the representative array factor plots in this section include the array factor using the measured offsets with no unknown offsets for reference as well as the actual array factor that uses the known measured offsets and unknown GPS errors. In Figure 2a, the unknown offsets distort the phases so that the phase compensation is not correct and the sidelobes increase (dashed red line). Figure 2b shows a similar setup with the unknown offsets set to zero so that there is only known measurement offsets. In this case, the sidelobe levels increase because the Dolph-Chebyshev are designed for a ULA.

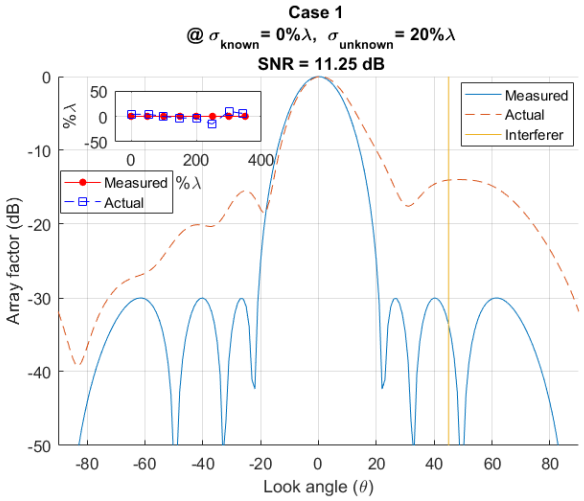

(a)

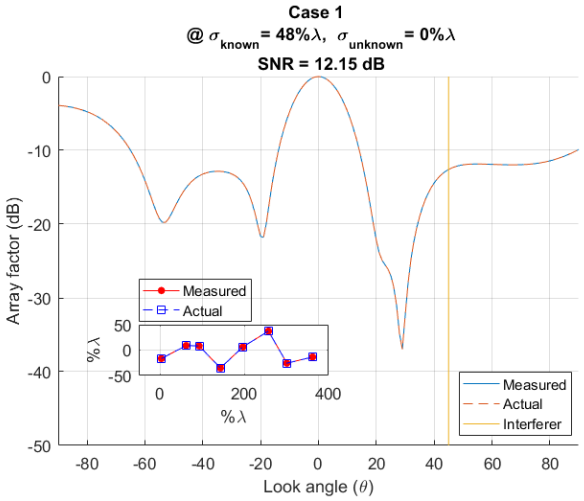

(b)

Fig. 2: Two example periodogram array factors: a) with no measured offset and b) with no unknown offset. In each plot, the array factor using measured (blue) and actual (red) offsets is shown. The inset shows measured (red circle) and actual (blue square) positions for the $P = 8$ sensor array used in this simulation run.

B. Case 2: MVDR Using Data Covariance

Case 2 is the standard MVDR algorithm. The DCM is used for the signal covariance matrix $\mathbf{R}_{xx}$. In this case the algorithm is often called Minimum Power Distortionless Response (MPDR). The weights are

$$\vec{w} = \frac{\mathbf{R}_{xx}^{-1}\mathbf{A}_1}{\mathbf{A}_1^H\mathbf{R}_{xx}^{-1}\mathbf{A}_1}. \tag{5}$$

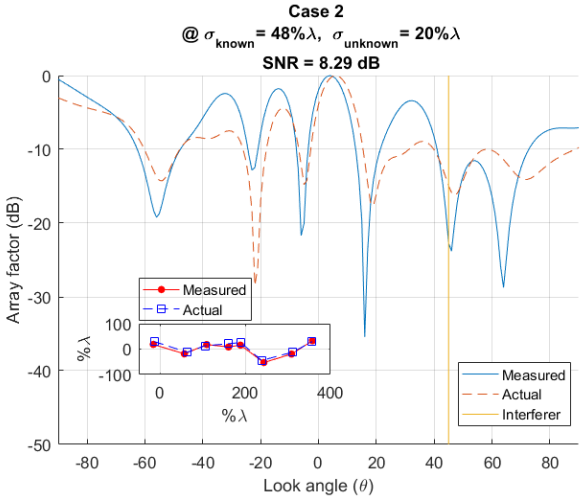

Fig. 3: An example MVDR array factor for estimated and actual offsets. The inset shows estimated and actual positions for the $P = 8$ element array used in this simulation run.

The measured offsets are used for the desired signal's steering vector $\mathbf{A}_1$ to calculate the weights, but the weights are applied to the actual array factor (which includes unknown errors) from which the SNR is calculated. An array factor plot shown in Figure 3 was generated to represent an output of this process. In both patterns, there is a null at the interferer and the desired signal is aligned with a lobe. However, even with 100 snapshots for the DCM estimate, there are several very high correlation lobes with the worst at -90°.

The MVDR algorithm's performance is dependent on the number of snapshots that are used to estimate the DCM. In some cases, prior knowledge of the DCM is available and may allow it to be estimated more accurately. In consideration of this, we also run a special case of the MVDR algorithm where the data covariance matrix is analytically derived using the measured offsets and assuming perfect knowledge of the sources and noise statistics (including the sources' directions of arrival). This case represents an upper bound on performance and is analogous to infinite snapshots.

C. Case 3: Generalized Sidelobe Canceller

The Generalized Sidelobe Canceller (GSC) is a variation of MVDR that can include additional linear constraints [16]. In this case, we add additional constraints to place nulls at the known directions of arrival for the clutter. Note that even though we assume knowledge of the clutter angles, unknown offsets will still create errors in the clutter suppression.

The first step is to define the linear constraint equation:

$$\mathbf{C}^H\vec{w} = \vec{g}, \tag{6}$$

where $\vec{g} = \begin{bmatrix} 1 & 0 \end{bmatrix}^T$ or $\vec{g} = \begin{bmatrix} 1 & 0 & 0 \end{bmatrix}^T$ for the distortionless followed by the null constraints and $\mathbf{C} = \begin{bmatrix}\mathbf{A}_1 \mid \mathbf{A}_{2:Q}\end{bmatrix}$ is comprised of the desired signal steering vector, $\mathbf{A}_1$, and the clutter steering vectors, $\mathbf{A}_{2:Q}$.

The weight vector is then

$$\vec{w} = \left[\mathbf{I} - \mathbf{C}_a(\mathbf{C}_a^H\mathbf{C}_a)^{-1}\mathbf{C}_a^H\right]\mathbf{C}(\mathbf{C}^H\mathbf{C})^{-1}g, \tag{7}$$

where $\mathbf{I}$ is the identity matrix and $\mathbf{C}_a$ is the orthogonal complement of $\mathbf{C}$, such that $\mathbf{C}_a^H\mathbf{C} = 0$ and $\mathbf{C}_a$ spans the null space of $\mathbf{C}$.

A representative array factor plot for this case is presented in Figure 4. The array factor for the measured offsets has a perfect null at the interferer, but still suffers from the high correlation lobes at other angles (as in Case 2) due to insufficient snapshots. In this particular run, even the main lobe no longer aligns with the desired signal direction. The number of snapshots needs to be 1000 before SNR degradation is reduced to only 1 to 2 dB for this particular setup. When the unknown offsets are included in the signal model, the null is smoothed and the performances drop further. Although the particular instantiations in this section show Case 2 outperforming Case 3 in terms of SNR, we will show in the following section that Case 3 does generally outperform Case 2 for these parameters.

Case 3 requires perfect knowledge of the incident clutter angles. It is meant to represent the best case situation where surface scattering can be predicted by an accurate digital elevation model, which is not always the case because the clutter can come from englacial targets and/or the digital elevation model may not be sufficiently accurate. In these situations, we would estimate the clutter angle from the data using direction of arrival estimation. We assume that the performance of the GSC algorithm would drop in this case so the results presented represent an upper bound on performance.

III. Results and Discussion

To better understand the performance limits, we first compute the minimum and maximum SNR that we expect to achieve. Given the noise variance of 0.1 and the clutter and desired unity variance, the SNR for a single sensor is $SNR = 1/(0.1 + 1) = -0.4$ dB. If the weights of the filter are fully randomized and independent to the sources and noise, then we expect the array gain to be 0 dB and the array output to have the same SNR as for a single channel: ~ -0.4 dB. The maximum SNR with perfect noise suppression is $P \times 1/0.1$. For $P = 8$, this is 19 dB, and for $P = 3$, this is 14.8 dB. Quasi-perfect noise suppression is possible when the clutter and desired sources have low enough correlation. This is usually the case for ice sounding radar because of the wide angular separation between the clutter and the desired nadir return.

The baseline periodogram results are shown in Figure 5. Here we see some expected trends. For $P = 8$, the peak SNR of 18 dB is obtained for the zero measured offset and zero

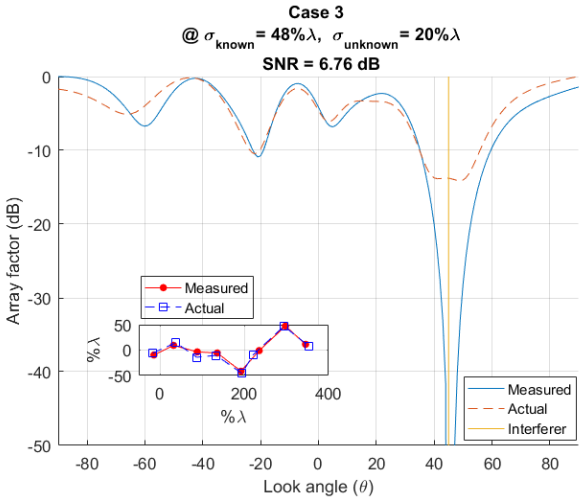

Fig. 4: Example GSC array factor for measured and actual offsets. The inset shows measured and actual positions for the $P = 8$ sensor array used in this simulation run.

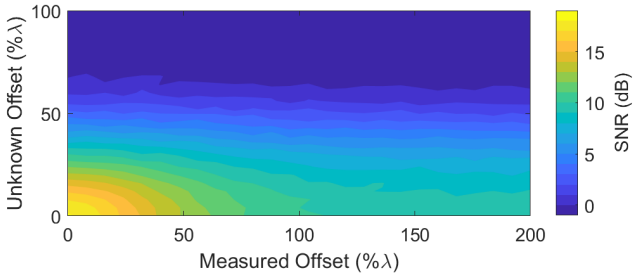

(a) SNR for $P = 8$ sensors.

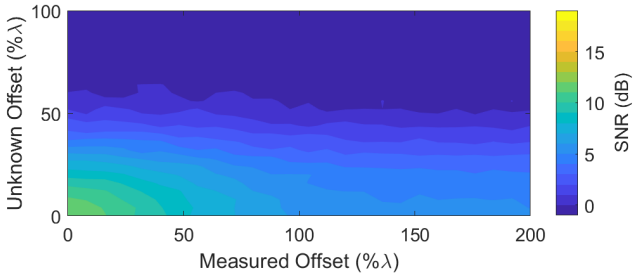

(b) SNR for $P = 3$ sensors.

Fig. 5: Periodogram results for a) $P = 8$ and b) $P = 3$ sensors.

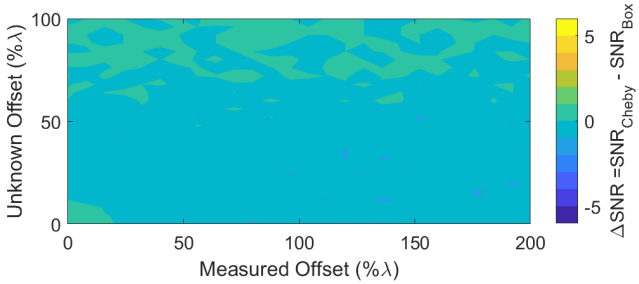

Fig. 6: Chebyshev and boxcar comparison with $P = 8$ sensors.

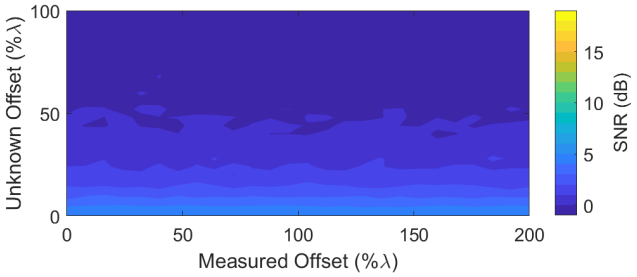

(a) SNR for P=8 sensors and M=20 snapshots.

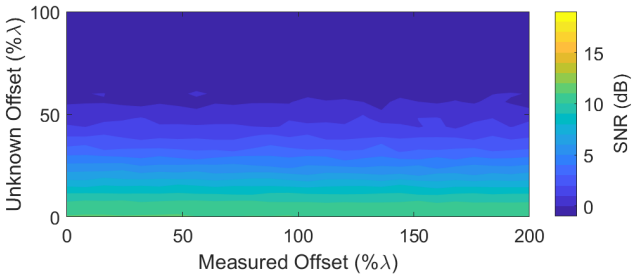

(b) SNR for P=8 sensors and M=100 snapshots.

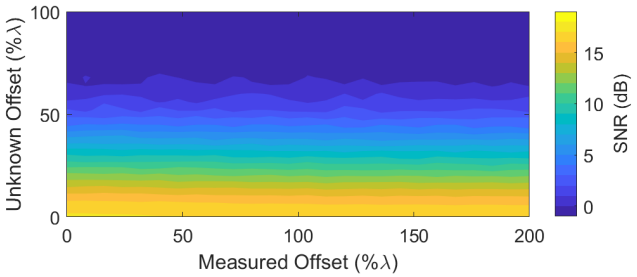

(c) SNR for P=8 sensors and M=1000 snapshots.

Fig. 7: MVDR SNR for varying numbers of snapshots. Note the lack of dependence on the measurement offset.

unknown offset case. This is slightly less than 19 dB because the windowing introduces a slight mismatch with the desired signal and the noise is not as effectively averaged down as with a boxcar window. However, the Chebyshev window improves the clutter suppression over the boxcar window. The simulation is repeated with a boxcar window and the difference in SNR is plotted, as shown in Figure 6. The difference in Figure 6 is about 0.5 dB in favor of the Chebyshev window for low levels of offset. However, boxcar is favored by 0.5 dB for any offsets above $15\%\lambda$. For the $P = 3$ case, the clutter falls within the mainlobe (not shown) and the peak SNR is less than 12 dB. For larger clutter angles that fall outside the main lobe, the performance approaches the maximum as with $P = 8$. Finally, with highly randomized measurement offsets, the difference in windowing is negligible with the boxcar slightly outperforming the Chebyshev due to the improved variance reduction of uniform weights. For $P = 8$ the SNR plateaus at 9 dB and 5 dB for $P = 3$, which matches the expected averaging power of the array of $10log_{10}P$. In all cases, the SNR drops off uniformly and rapidly with unknown offset errors.

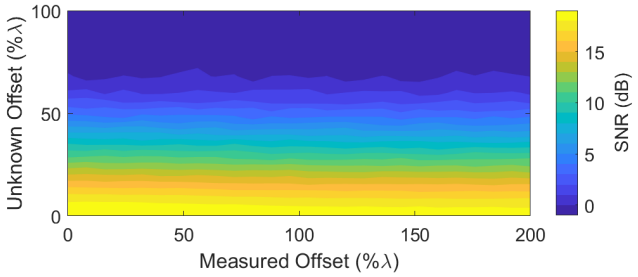

(a) $P = 8$

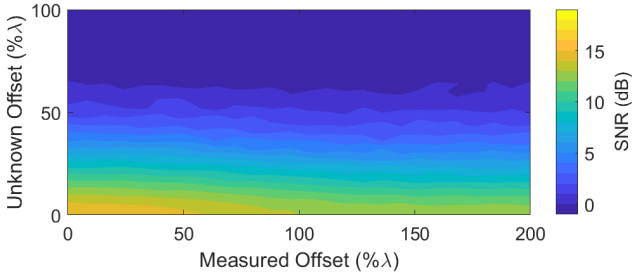

(b) $P = 3$

Fig. 8: MVDR with analytically generated DCM for a) $P = 8$ sensors and b) $P = 3$ sensors.

Figure 7 shows the MVDR results for three different snapshots scenarios and $P = 8$ sensors. We find that the performance of the algorithm does not depend on the measured offset. This is convenient as the measured offsets tend to be substantially larger than the unknown offsets; they are also likely to be a significant fraction of the wavelength for typical ice sounding frequencies [17]. The same pattern was found when the simulations were repeated with two clutter sources. As with the periodogram, SNR drops uniformly with increasing unknown offsets and this was also observed with two clutter sources.

While lack of dependence on measured offsets is useful, the MVDR algorithm performs significantly worse than the non-adaptive periodogram for $M = 20$ snapshots. This is due to the well-known self-nulling effect (e.g. [10]). MVDR has similar performance around $M = 100$ snapshots, but is only better for larger random measured offsets. Therefore, traditional MVDR has low performance over the range of snapshots that are likely to be available for ice sounding. Even with $M = 1000$ snapshots, the periodogram outperforms MVDR by 1 dB for zero offsets. However, MVDR performance is significantly better for non-zero measured offsets. This suggests that an improved DCM, MVDR could offer substantial gains over the periodogram method.

Self-nulling becomes worse as the desired signal power increases. For our low snapshot case of $M = 20$, we find that the output SNR does not change substantially for desired source powers ranging from 0.1 to 100: all provide an SNR between 4-5 dB for zero unknown offsets with performance independent of the measured offset. As snapshots increase, the resultant SNR becomes increasingly dependent on the relative

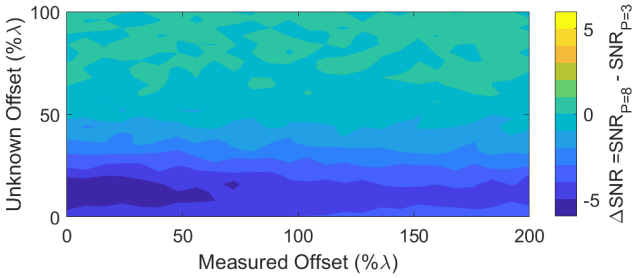

(a) M=20

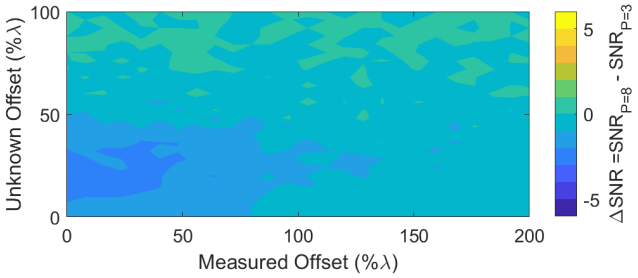

(b) M=100

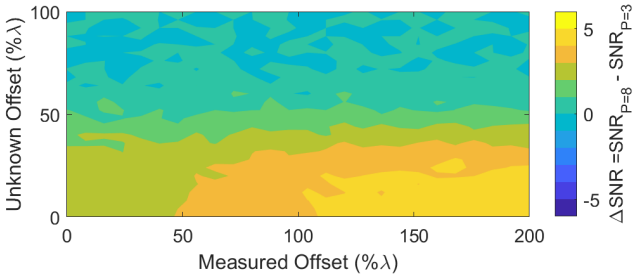

(c) M=1000

Fig. 9: SNR Difference in MVDR SNR performance between $P = 8$ sensors and $P = 3$ sensors.

signal power as one expects. We show the limiting case of this in Figure 8. Here, the DCM is generated analytically with perfect knowledge of the noise, source statistics, and their directions of arrival. The offsets are still treated as before. In this figure, the peak SNR is 19 dB for $P = 8$ and 14.8 dB for $P = 3$ – in other words, the expected ideal performance.

Another property of self-nulling is that the number of snapshots required to reduce its impact grows nonlinearly with increases in the number of sensors. This leads to an interesting phenomenon where smaller sensor arrays may outperform larger sensor arrays if we use the entire arrays coherently. Figure 9 compares the performance of the $P = 3$ MVDR result to the $P = 8$ result. For the number of snapshots typically available to ice sounding, the three sensor array outperforms the eight sensor array.

Another interesting trend in Figure 9 is that the performance of the $P = 3$ sensor MVDR is slightly dependent on measured offset. We attribute this to the increased probability that the clutter and source will be highly correlated when the positions are randomized;the array is small and unfortunate combinations of highly correlated phase shifts will be more

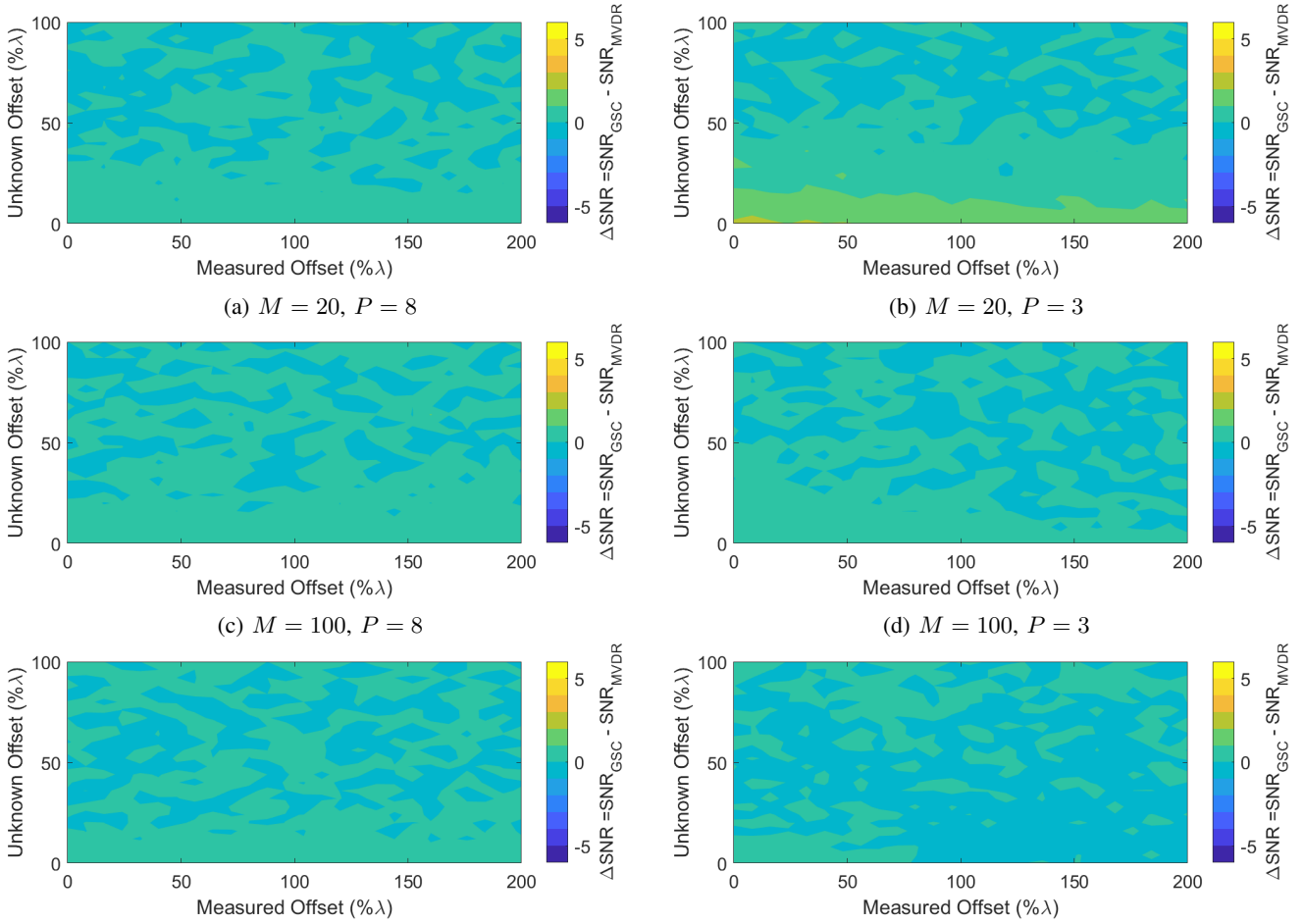

(a) $M = 20$, $P = 8$

(b) $M = 20$, $P = 3$

(c) $M = 100$, $P = 8$

(d) $M = 100$, $P = 3$

(e) $M = 1000$, $P = 8$

(f) $M = 1000$, $P = 3$

Fig. 10: SNR Difference between the GSC and MVDR algorithms for $P = 8$ and $P = 3$ sensors.

likely.

The results of the GSC compared with the corresponding MVDR results are shown in Figure 10. Here the SNR performance of MVDR is subtracted from the GSC SNR. Even with perfect knowledge of the direction of arrival, the benefits of the generalized sidelobe canceller are very small (around 1 dB) for $P = 8$ and are only apparent for low unknown offsets. This was the case for two clutter sources as well.

The situation is better and worse for the smaller $P = 3$ sensor array. For low snapshots, the null placement gains 2-3 dB of SNR. As snapshots increase, this performance boost drops and eventually becomes negative for $M = 1000$ snapshots and large measured offsets. The performance of the GSC also drops with increased measured offsets for $P = 3$ sensors. We attribute this to the same reason as before: the increased probability of correlation. For the case of two clutter sources, the GSC performance drops significantly for large measured offsets; we assume the cause of this is due to the over constrained problem and the probability of high correlation with the desired source.

IV. Conclusion

We have evaluated how known and unknown position errors affect beamforming with the periodogram and two variations of the MVDR algorithm. These results can be used to evaluate system requirements and specifications for future multipass or swarm/constellation data collection scenarios. In both MVDR (somtimes called MPDR) variations, the DCM used to determine the beamforming weights includes both the desired and interfering signals [10]. The signal model includes a desired ice bottom source from nadir that is broadside to the array and one or two surface clutter sources.

The primary conclusion is that known *measured offsets* can be tolerated very well by MVDR as long as the number of sensors is sufficiently higher than the number of clutter sources; however, MVDR requires a large number of snapshots relative to the number of sensors. This result makes sense because the MVDR array gain is known to be a function only of the correlation between the desired signal and the interference [10]. For a small number of sensors with offsets between $0\%\lambda$ to $50\%\lambda$, SNR performance can improve by up to 3 dB due the increased probability of higher correlation. Above $50\%\lambda$, the phases are already fully randomized so that

increased flight path errors do not affect the SNR. For a large number of sensors, the average correlation does not change with respect to $\%\lambda$, and there is negligible dependence on flight path error. However, a large number of sensors requires more snapshots to obtain good performance to avoid self-nulling; the $P = 3$ sensor array's MVDR SNR is higher than the $P = 8$ sensor array for typical numbers of snapshots used in ice sounding despite having much fewer sensors.

Since snapshots are limited in radar applications and seem to be the primary barrier for MVDR to operate in the presence of flight path variations, we recommend future efforts focus on evaluating how position offsets affect robust adaptive beamforming methods (for example [18]) that handle poor DCM estimates or improve DCM estimation. Some methods (such as forward-backward averaging and spatial smoothing with subarrays) are generally not applicable to these randomized array geometries. Since the surface clutter geometry may be well known, applications of fixed or estimated nulls should also be considered [3].

The second conclusion is that *unknown offsets* are not mitigated by any of the algorithms investigated, and there is very little discrepancy between the scenarios tested so that each is equally poor. This result illustrates the importance of accurate relative position knowledge for array processing. If a known single target dominates the response, this could be used to calculate the relative positions and provide a correction for the nadir steering vector. A smooth ice surface return estimated from an accurate digital elevation model is a potential candidate.

V. Acknowledgements

This work was funded by NSF 1739003 and the University of Kansas.

References

[1] F. Rodriguez-Morales, S. Gogineni, C. J. Leuschen, J. D. Paden, J. Li, C. C. Lewis, B. Panzer, D. G.-G. Alvestegui, A. Patel, K. Byers *et al.*, "Advanced multifrequency radar instrumentation for polar research," *IEEE Transactions on Geoscience and Remote Sensing*, vol. 52, no. 5, pp. 2824–2842, 2014.

[2] J. Li, J. Paden, C. Leuschen, F. Rodriguez-Morales, R. D. Hale, E. J. Arnold, R. Crowe, D. Gomez-Garcia, and P. Gogineni, "High-altitude radar measurements of ice thickness over the antarctic and greenland ice sheets as a part of operation icebridge," *IEEE Transactions on Geoscience and Remote Sensing*, vol. 51, no. 2, pp. 742–754, Feb 2013.

[3] U. Nielsen, J. Dall, S. S. Kristensen, and A. Kusk, "Coherent surface clutter suppression techniques with topography estimation for multi-phase-center radar ice sounding," in *EUSAR 2012; 9th European Conference on Synthetic Aperture Radar*. VDE, 2012, pp. 247–250.

[4] R. Scheiber, P. Prats-Iraola, M. Nannini, M. Villano, K. Morrison, and N. Gebert, "Comparison of digital beamforming techniques for enhanced ice sounding radar data processing," in *EUSAR 2014; 10th European Conference on Synthetic Aperture Radar*, June 2014, pp. 1–4.

[5] P. S. Tan, J. Paden, J. Li, J.-B. Yan, and P. Gogineni, "Robust adaptive mvdr beamforming for processing radar depth sounder data," in *2013 IEEE International Symposium on Phased Array Systems and Technology*, October 2013, pp. 622–629.

[6] J. A. Vincent and E. J. Arnold, "Beamforming sensitivity of airborne distributed arrays to flight tracking and vehicle dynamics," in *2017 IEEE Aerospace Conference*, March 2017, pp. 1–14.

[7] C. Leuschen, R. Hale, S. Keshmiri, J. B. Yan, F. Rodriguez-Morales, A. Mahmood, and S. Gogineni, "Uas-based radar sounding of the polar ice sheets," *IEEE Geoscience and Remote Sensing Magazine*, vol. 2, no. 1, pp. 8–17, March 2014.

[8] P. Gogineni, C. R. Simpson, J. Yan, C. R. O'Neill, R. Sood, S. Z. Gurbuz, and A. C. Gurbuz, "A cubesat train for radar sounding and imaging of antarctic ice sheet," in *IGARSS 2018 - 2018 IEEE International Geoscience and Remote Sensing Symposium*, July 2018, pp. 4138–4141.

[9] L. C. Godara, "Application of antenna arrays to mobile communications. ii. beam-forming and direction-of-arrival considerations," *Proceedings of the IEEE*, vol. 85, no. 8, pp. 1195–1245, 1997.

[10] H. L. Van Trees, *Optimum array processing: Part IV of detection, estimation, and modulation theory*. John Wiley & Sons, 2004.

[11] E. J. Arnold, J.-B. Yan, R. D. Hale, F. Rodriguez-Morales, and P. Gogineni, "Identifying and compensating for phase center errors in wing-mounted phased arrays for ice sheet sounding," *IEEE Transactions on Antennas and Propagation*, vol. 62, no. 6, pp. 3416–3421, 2014.

[12] B. Miller and E. J. Arnold, "Wing-integrated airborne antenna array beamforming sensitivity to wing deflections," in *2018 IEEE Aerospace Conference*, March 2018, pp. 1–11.

[13] K. Gustafsson, F. McCarthy, and A. Paulraj, "Mitigation of wing flexure induced errors for airborne direction-finding applications," *IEEE transactions on signal processing*, vol. 44, no. 2, pp. 296–304, 1996.

[14] J. Petko and D. Werner, "Positional tolerance analysis and error correction of micro-uav swarm based antenna arrays," in *2009 IEEE Antennas and Propagation Society International Symposium*. IEEE, 2009, pp. 1–4.

[15] A. Adrian, *System performance and performance enhancement relative to element position location errors for distributed linear antenna arrays*. Michigan State University, 2014.

[16] S. S. Haykin, *Adaptive filter theory*. Pearson Education India, 2008.

[17] E. Arnold, F. Rodriguez-Morales, J. Paden, C. Leuschen, S. Keshmiri, S. Yan, M. Ewing, R. Hale, A. Mahmood, A. Blevins *et al.*, "Hf/vhf radar sounding of ice from manned and unmanned airborne platforms," *Geosciences*, vol. 8, no. 5, p. 182, 2018.

[18] S. A. Vorobyov, "Principles of minimum variance robust adaptive beamforming design," *Signal Processing*, vol. 93, no. 12, pp. 3264–3277, 2013.